Biophysical Journal, Volume *117*

Supplemental Information

NMR Structural Analysis of Isolated *Shaker* Voltage-Sensing Domain in LPPG Micelles

Hongbo Chen, Junkun Pan, Disha M. Gandhi, Chris Dockendorff, Qiang Cui, Baron Chanda, and Katherine A. Henzler-Wildman

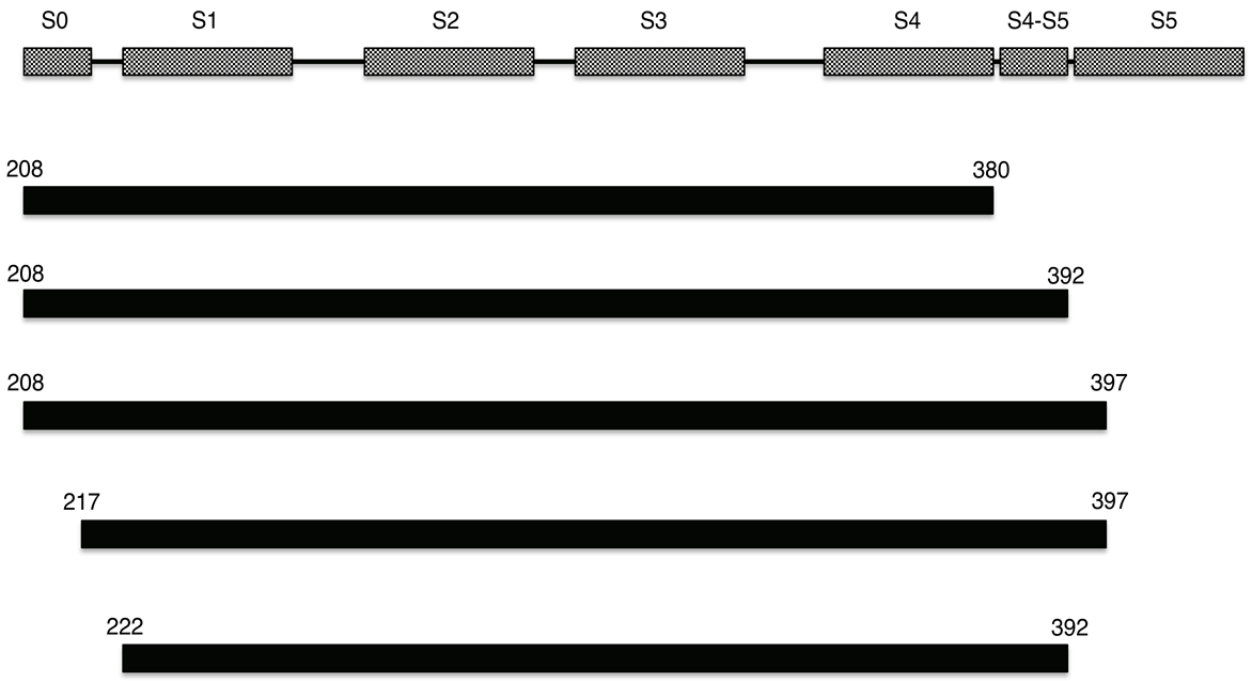

Figure S1. Constructs screened for optimizing Shaker-VSD expression. The highest expressing construct (217-397) was chosen for further NMR studies.

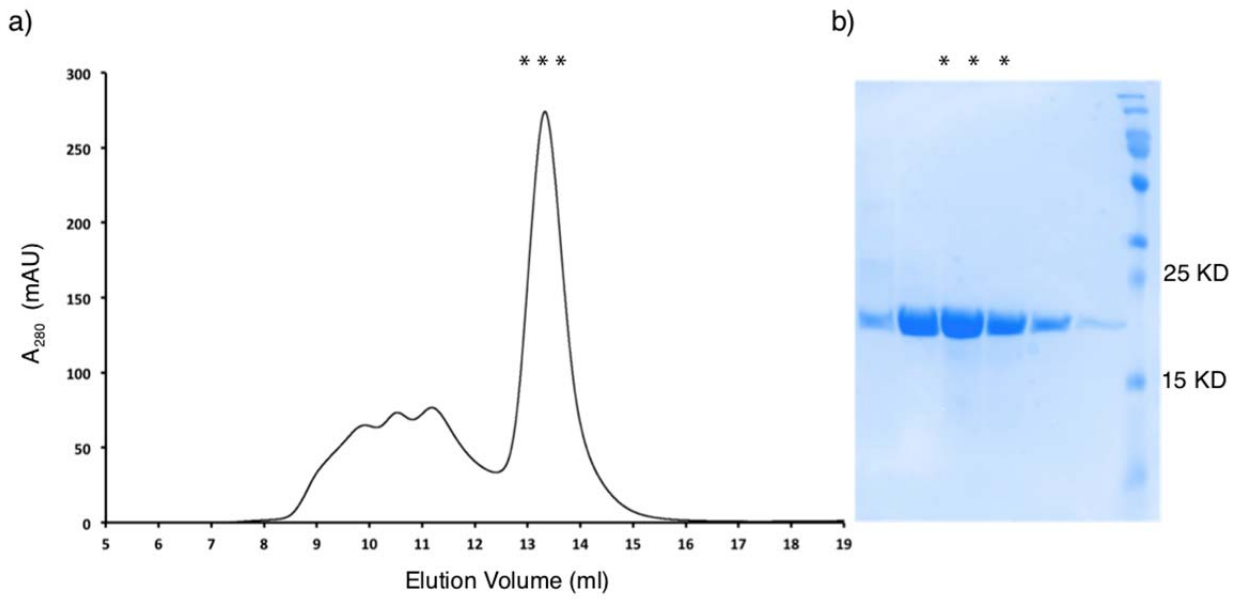

Figure S2. Shaker-VSD purification. (a) Representative gel filtration elution profile of the isolated Shaker-VSD in 0.2% LPPG on a Superdex 200 column. (b) SDS-PAGE gel of fractions from the main peak of the S200 elution profile for the isolated Shaker-VSD shows that the purified protein is a monomer with an apparent molecular mass near 20 kDa as expected.

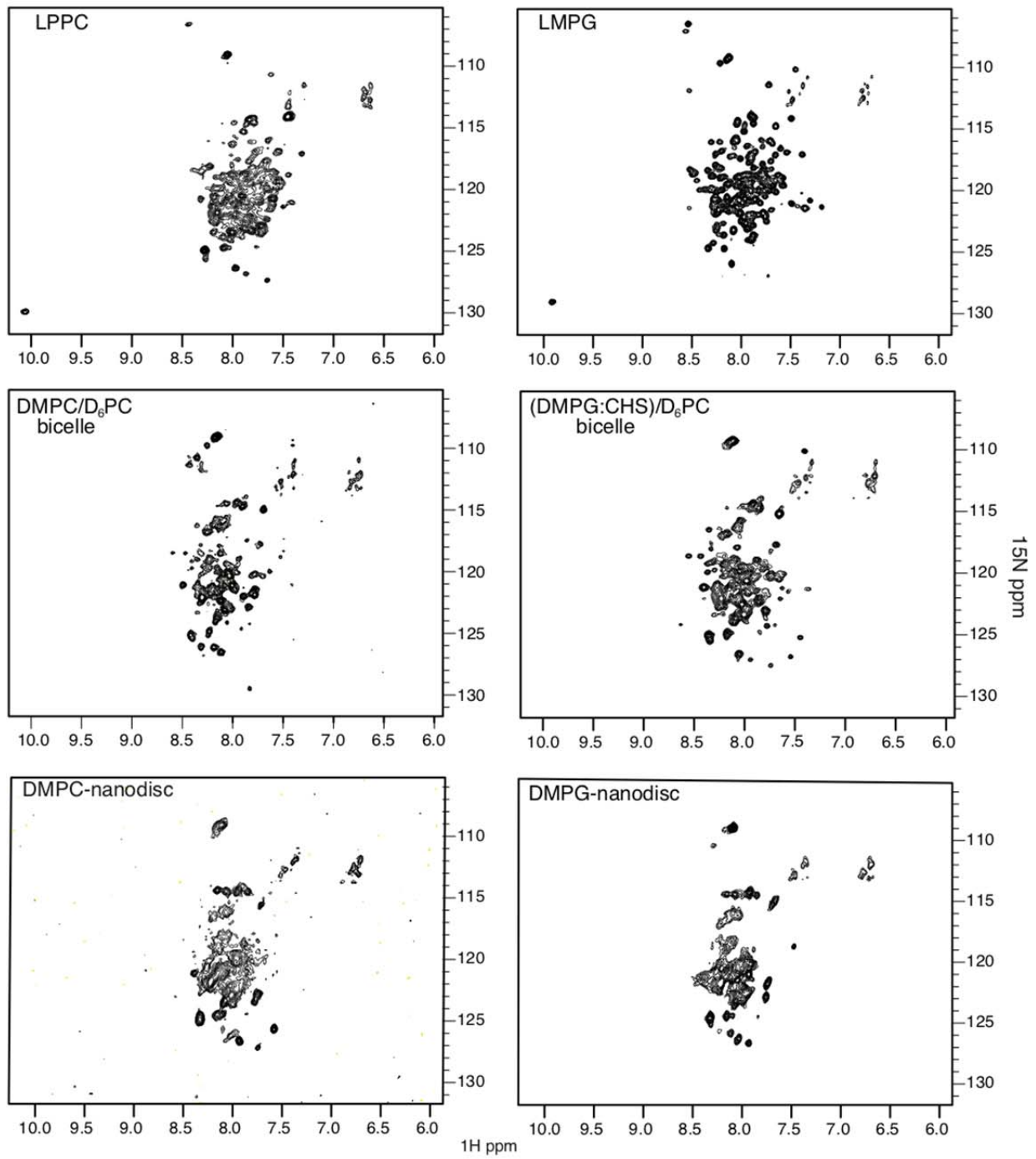

Figure S3. Representative ^{1}H-^{15}N TROSY-HSQC spectra of the isolated Shaker-VSD at pH 7.0 in different membrane mimetics tested during NMR sample optimization. All spectra were acquired on a 750MHz Bruker magnet at 45 °C, except for the DMPC/D_6PC bicelle sample, which was acquired at 37 °C.

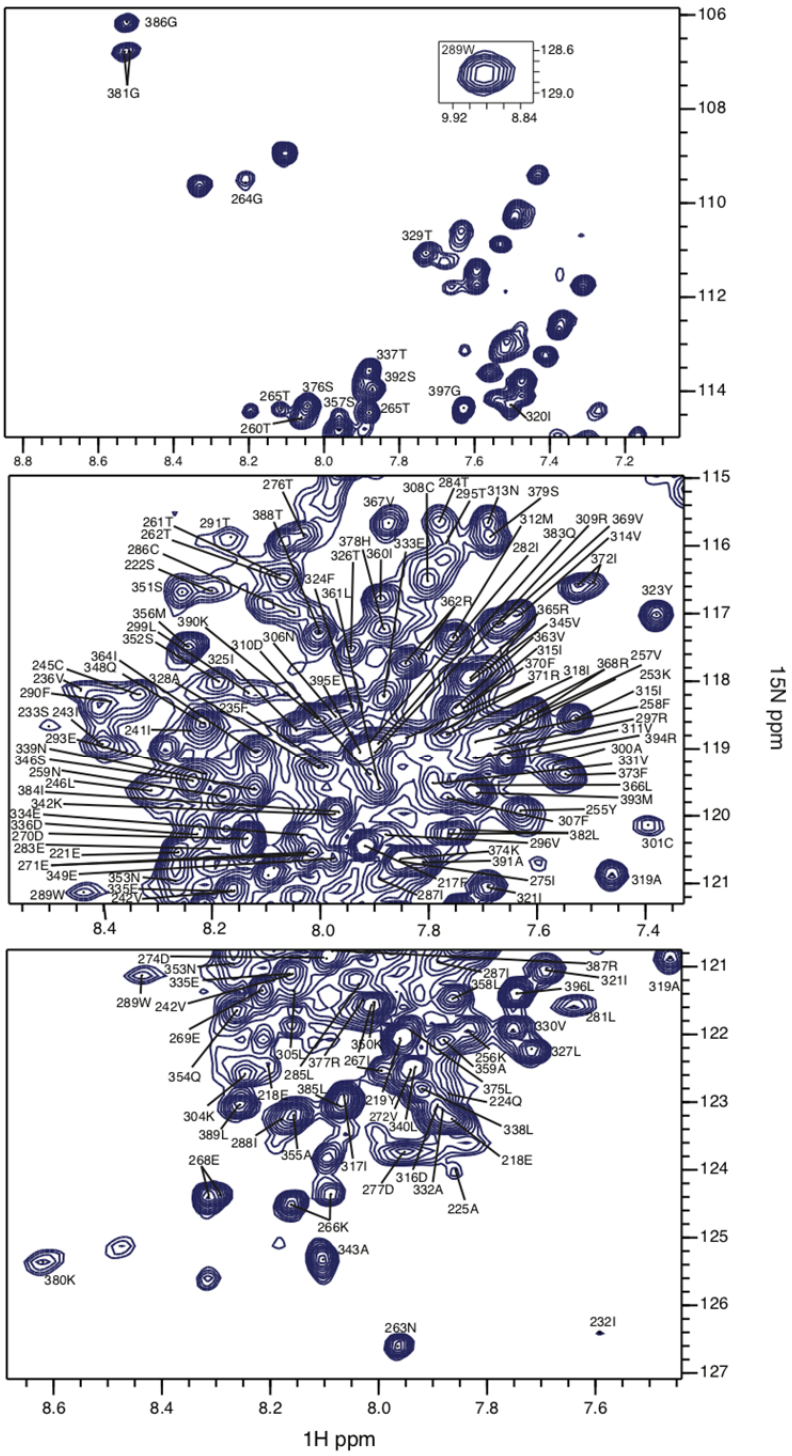

Figure S4. ^{1}H-^{15}N NMR chemical assignments of isolated Shaker-VSD at 45°C in 1.6% LPPG at pH 7.0.

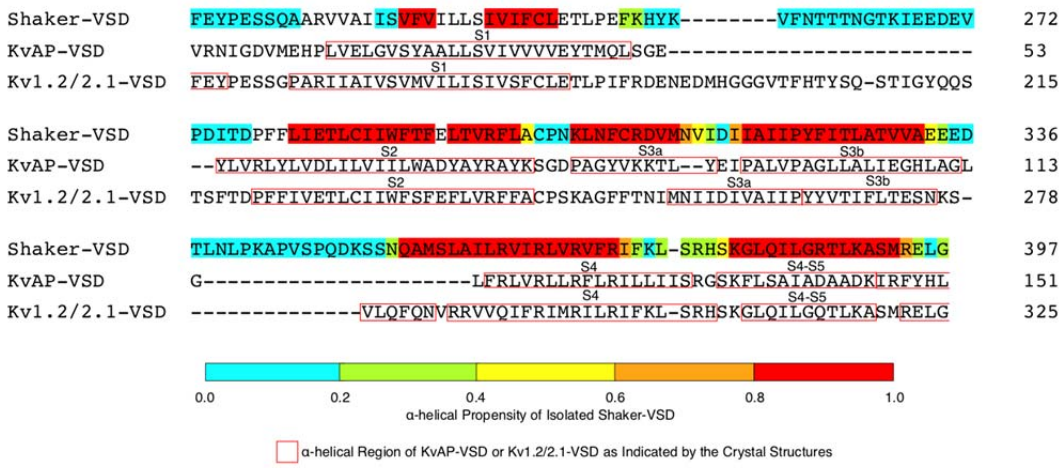

Figure S5. Comparison of secondary structures of isolated Shaker-VSD, KvAP-VSD and Kv1.2/2.1-VSD. The sequence of Shaker-VSD, KvAP-VSD and Kv1.2/2.1-VSD are aligned with Clustal Omega and manually adjusted. The α-helical propensity of isolated Shaker-VSD based on its backbone chemical shifts as shown in Figure 2 is plotted on its sequence with a cyan to red color scale indicating the location of helical regions (0 indicating 0% tendency to form α helix while 1 indicating 100% tendency). Residues in Shaker-VSD without color indicate lack of backbone assignment. Helical regions of KvAP-VSD and Kv1.2/2.1-VSD are marked with red rectangles based on their crystal structures (1ORQ and 2R9R) (1,2). The secondary structural features of isolated Shaker-VSD generally agrees with that of Kv1.2/2.1-VSD, except for S2-S3 linker and S3 transmembrane helix, which is more similar to KvAP-VSD.

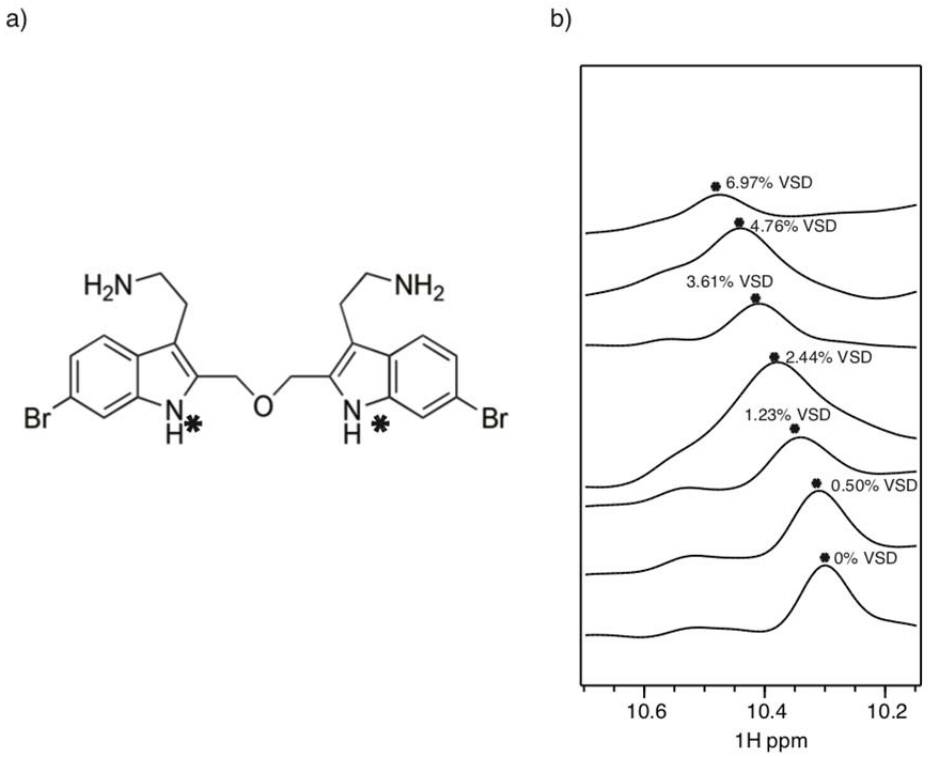

Figure S6: NMR titration of BrET with Shaker-VSD. (a) Structure of BrET with indole marked with *. Stacked plot of 1D ^{1}H NMR spectra of BrET with increasing concentration of added Shaker-VSD in the region of 10ppm. The chemical shift change of the peak corresponding to the BrET indole proton (*) upon Shaker-VSD titration shown in this figure was used to generate the binding curve in Fig. 3.

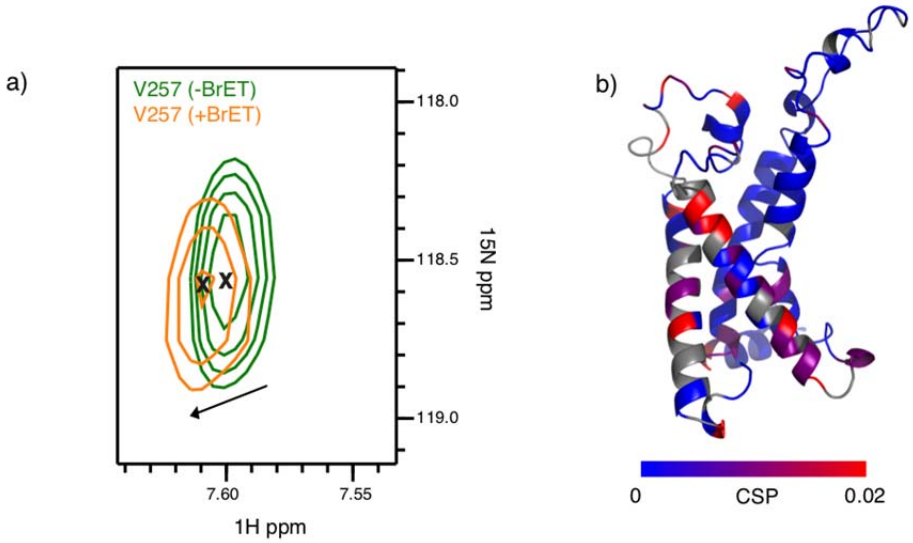

Figure S7. Effect of BrET binding as observed from the NMR spectrum of Shaker-VSD. (a) Overlay of the peak corresponding to Val257 in Shaker-VSD from a TROSY-HNCO spectrum without BrET (green) and with BrET (orange). The chemical shift perturbation is about 0.026. (b) Chemical shift perturbations are plotted on a homology model of isolated Shaker-VSD with a blue to red color scale. Small chemical shift perturbations are observed in many sites across the Shaker-VSD, suggesting that the protein undergoes a global conformational change upon binding.

Figure S8. Residues of Shaker-VSD exhibiting peak doubling in the well-resolved 3D TROSY-HNCO or TROSY-HNCA NMR spectra are highlighted in orange.

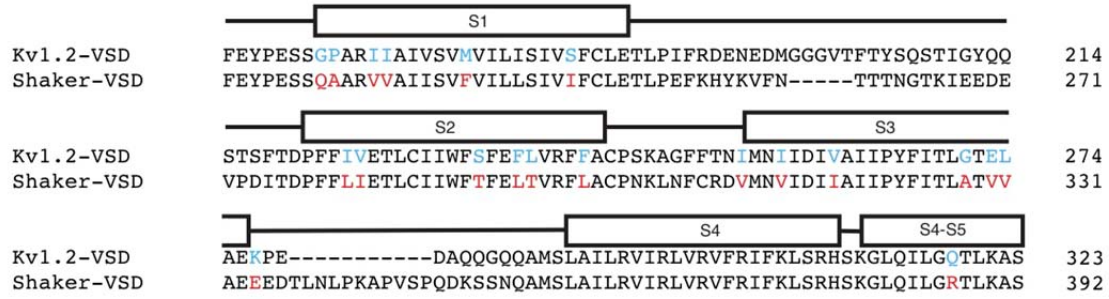

Figure S9: Sequence alignment of Kv1.2-VSD and Shaker-VSD. Residues in the transmembrane helices with different sequence are colored in red and blue.

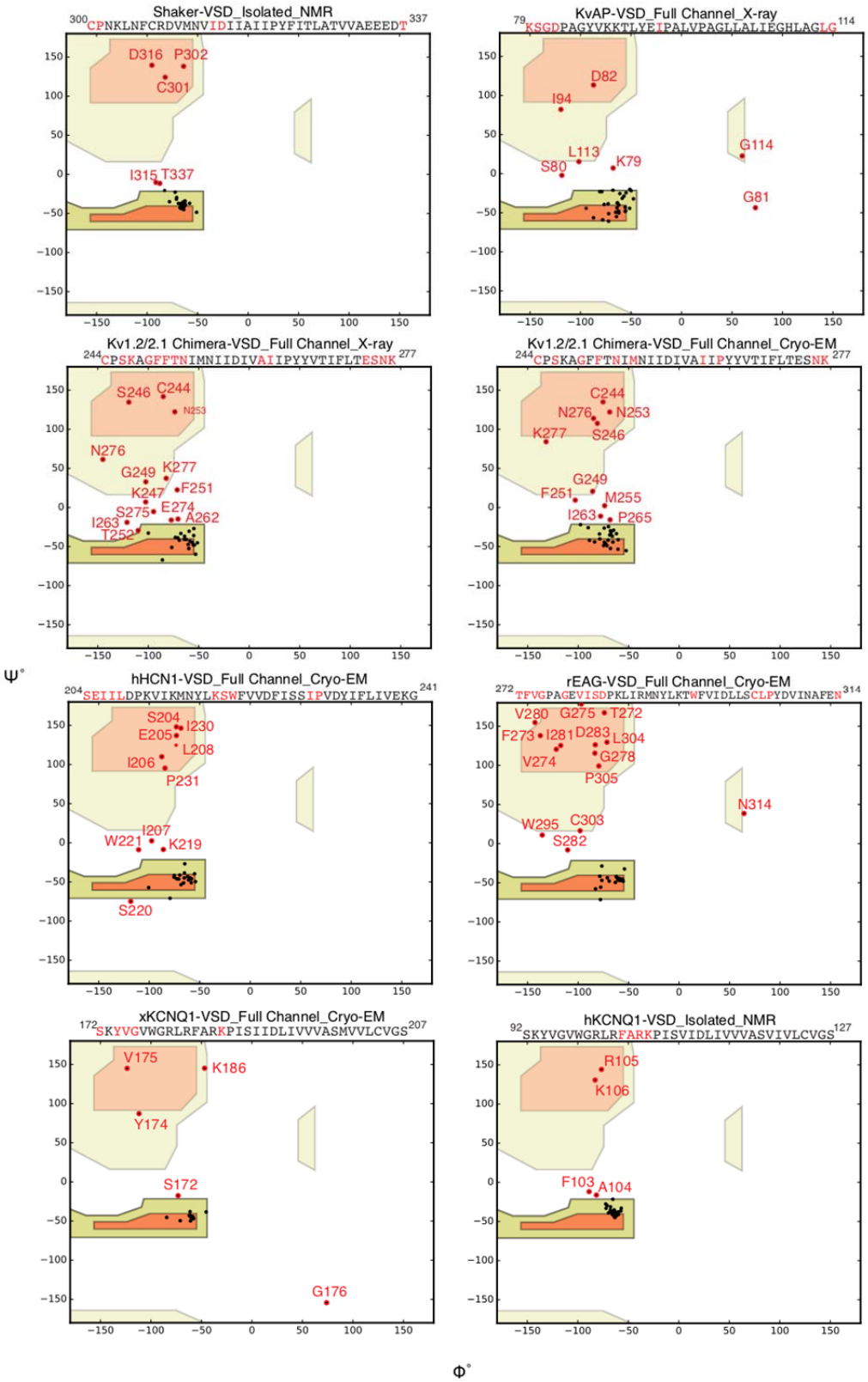
Shaker-VSD_Isolated_NMR
300 CPNKLNFCRDVMNVIDIIAIIPYFITLATVVAEEEDT 337
D316
P302
C301
I315
T337
KvAP-VSD_Full Channel_X-ray
79 KSGDPAGYVKKTLYEIPALVPAGLLALIEGHLAGLG 114
D82
I94
L113
S80
K79
G114
G81
Kv1.2/2.1 Chimera-VSD_Full Channel_X-ray
244 CPSKAGFFTNIMNIIDIVAIIPYYVTIFLTESNK 277
S246
C244
N253
N276
G249
K277
K247
F251
S275
E274
I263
A262
T252
Kv1.2/2.1 Chimera-VSD_Full Channel_Cryo-EM
244 CPSKAGFFTNIMNIIDIVAIIPYYVTIFLTESNK 277
C244
N276
N253
K277
S246
G249
F251
M255
I263
P265
hHCN1-VSD_Full Channel_Cryo-EM
204 SEIILDPKVIKMNYLKSWFVVDFISSIPVDYIFLIVEKG 241
S204
I230
E205
L208
I206
P231
I207
W221
K219
S220
rEAG-VSD_Full Channel_Cryo-EM
272 TFVGPAGEVISDPKLIRMNYLKTWFVIDLLSCLPYDVINAFEN 314
V280
G275
T272
F273
I281
D283
L304
V274
G278
P305
N314
W295
C303
S282
xKCNQ1-VSD_Full Channel_Cryo-EM
172 SKYVGVWGRLRFARKPISIIDLIVVVASMVVLCVGS 207
V175
K186
Y174
S172
G176
hKCNQ1-VSD_Isolated_NMR
92 SKYVGVWGRLRFARKPISVIDLIVVVASVIVLCVGS 127
R105
K106
F103
A104
Ψ°
Φ°

Figure S10: Ramachandran plots of the backbone dihedral angles of the S2-S3 linker and S3 helix in different Kv-VSDs. Backbone φ and ψ angles are extracted from the deposited PDB structures and/or data in the following references: isolated Shaker-VSD (our NMR results); KvAP-VSD in full channel, X-ray (1ORQ) (1); Kv1.2/2.1-VSD in full channel, X-ray (2R9R) (2); Kv1.2/2.1-VSD in full channel, Cryo-EM (6EBK) (3); human KCNQ1-VSD, NMR (calculated with TALOS+ using backbone resonances assignment deposited in BMRB: 19708) (4); *Xenopus laevis* KCNQ1-VSD in full channel, cryo-EM (5VMS) (5); EAG-VSD in full channel, cryo-EM (5K7L) (6); HCN1-VSD in full channel, cryo-EM (5U6O) (7). The ramachandran plot is generated based on theoretical definition of backbone φ and ψ angles in different secondary structural configurations (8), with intense color indicating right-handed helix (orange color indicating favored and yellow indicating allowed regions) and pale orange and pale yellow indicating favored and allowed regions for other secondary structures. Non-helical residues are labeled in red. These analyses were used to define the secondary structure configuration of Shaker-VSD in Figure 5.

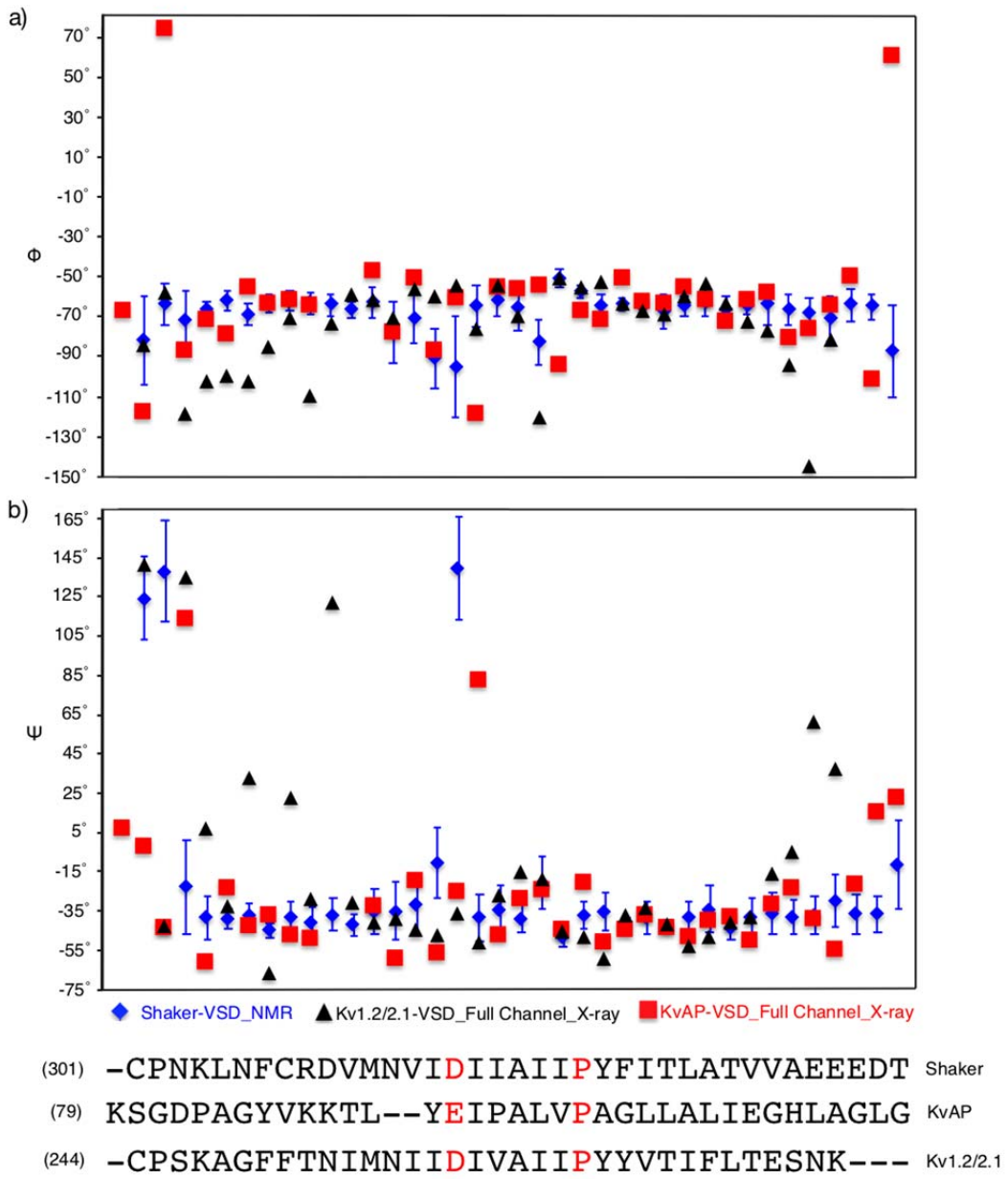

Figure S11: Comparison of backbone dihedral angles of Shaker-VSD, full-lenth KvAP and Kv1.2/2.1 in the S2-S3 linker and S3 helix. Backbone φ and ψ angles are extracted from the deposited PDB structures and/or data in the following references: isolated Shaker-VSD (our NMR results); KvAP-VSD in full channel, X-ray (1ORQ) (1); Kv1.2/2.1-VSD in full channel, X-ray (2R9R) (2). The φ and ψ angles distribution pattern of Shaker-VSD is more similar with that of full-length KvAP crystal structure then that full-length Kv1.2/2.1 crystal structure, indicating that some structural features of this region in Shaker-VSD might be more similar with that of KvAP.

Table S1. Membrane mimetics screened for VSD Reconstitution

Membrane Mimetics			^{15}N-^{1}H HSQC Spectrum Quality
Detergent Micelles	DM		Aggregate
	DDM		Failed to extract from membrane
	OG		Failed to extract from membrane
	CHAPS		Failed to extract from membrane
	Foscholine-12		Poor
	LMPG		Great
	LPPG		Great
	LPPC		OK
	LPPC:LPPG=1:1		OK
	LPPG:Chobimalt=4:1		OK
Bicelles	**Long-chain Lipids**	**Short-chain Lipids**	**^{15}N-^{1}H HSQC Spectrum Quality**
	DMPC	D6PC	Poor
	DMPC:DMPG=3:1	CHAPSO	Reconstitution failed
	POPC:POPG=3:1	D6PC	Poor
	POPC:POPA=3:1	D6PC	Poor
	POPE:POPG=3:1	D6PC	Poor
	DMPC:DMPA=3:1	D6PC	Poor
	DMPG	D6PC	Poor
	DMPG:Cholesterol=9:1	D6PC	OK
	DMPC:DMPA+1%PIP2	D6PC	Poor
	DMPC:DMEPC=3:1	D6PC	Poor
	DMPC:DMTAP=3:1	D6PC	Poor
	DMPG:Cholesterol=9:1	D7PC	OK
	DMPC:DMPA=3:1	D7PC	Poor
	DPPC	D7PC	Poor
	DPPG	D7PC	Poor
	DPPC:Choleterol=9:1	D7PC	Poor
	DPPG:Cholesterol=9:1	D7PC	OK
Nanodiscs	**Lipids**	**Scaffold Protein**	**^{15}N-^{1}H HSQC Spectrum Quality**
	DMPC	MSP1D1ΔH5	Poor
	DMPG	MSP1D1ΔH5	Poor
	DMPC:DMPA=3:1	MSP1D1ΔH5	Poor
Amphipol	A8-35		Poor

Supporting References:

1. Jiang, Y., Lee, A., Chen, J., Ruta, V., Cadene, M., Chait, B. T., and MacKinnon, R. (2003) X-ray structure of a voltage-dependent k+ channel. *Nature* **423**, 33-41
2. Long, S. B., Tao, X., Campbell, E. B., and MacKinnon, R. (2007) Atomic structure of a voltage-dependent k+ channel in a lipid membrane-like environment. *Nature* **450**, 376-382
3. Matthies, D., Bae, C., Toombes, G. E., Fox, T., Bartesaghi, A., Subramaniam, S., and Swartz, K. J. (2018) Single-particle cryo-em structure of a voltage-activated potassium channel in lipid nanodiscs. *Elife* **7**
4. Peng, D., Kim, J. H., Kroncke, B. M., Law, C. L., Xia, Y., Droege, K. D., Van Horn, W. D., Vanoye, C. G., and Sanders, C. R. (2014) Purification and structural study of the voltage-sensor domain of the human kcnq1 potassium ion channel. *Biochemistry* **53**, 2032-2042
5. Sun, J., and MacKinnon, R. (2017) Cryo-em structure of a kcnq1/cam complex reveals insights into congenital long qt syndrome. *Cell* **169**, 1042-1050 e1049
6. Whicher, J. R., and MacKinnon, R. (2016) Structure of the voltage-gated k(+) channel eag1 reveals an alternative voltage sensing mechanism. *Science* **353**, 664-669
7. Lee, C. H., and MacKinnon, R. (2017) Structures of the human hcn1 hyperpolarization-activated channel. *Cell* **168**, 111-120 e111
8. Ramachandran, G. N., Ramakrishnan, C., and Sasisekharan, V. (1963) Stereochemistry of polypeptide chain configurations. *J Mol Biol* **7**, 95-99